small NANO MICRO

Electrokinetics

Label-Free Attomolar Detection of Proteins Using Integrated Nanoelectronic and Electrokinetic Devices

*Jian-Ru Gong**

***H**igh-sensitivity screening of biomarkers is critical to areas ranging from early disease detection and diagnosis to bioterrorism surveillance. Here the development of integrated nanoelectronic and electrokinetic devices for label-free attomolar detection of proteins is reported. Electrically addressable silicon nanowire field-effect transistors and electrodes for electrokinetic transport are integrated onto a common sensor chip platform, and the nanowire devices are subsequently functionalized with receptors for selective biomarker detection. Nanowire devices modified with monoclonal antibody for prostate specific antigen exhibit close to a 10^4 increase in sensitivity due to streaming dielectrophoresis and corresponding electrostatic contribution to the binding affinity after application of an AC electric field. The devices are also modified with receptors for cholera toxin subunit B and achieve a similar enhancement. These results show general applicability of this method, and could open up opportunities in early stage disease detection and the analysis of proteins from single cells.*

Keywords:
- biosensors
- electrokinetics
- field-effect transistors
- nanotechnology
- nanowires

1. Introduction

High-sensitivity screening of proteins is critical in early cancer detection[1] and bioterrorism surveillance.[2] Unlike DNA samples, proteins can not be amplified easily by polymerase chain reaction (PCR),[3] highlighting the importance of protein detection at extremely low concentration. The semiconductor nanowire field-effect transistor (NWFET) has become a useful platform for direct electrical detection of biological species, due to the comparable size of NW diameter to that of biological species and excellent electrical signal of transducers.[4] The "bottom-up" silicon (Si) NW devices fabricated by the Lieber group have demonstrated applications for label-free, sensitive, and selective real-time detection of a wide range of biological species, including proteins,[5] nucleic acids[6] and viruses,[7] in either single-element or multiplexed formats. Similar detection limit is also reported for "top-down" fabrication methods of NW devices.[8] Although the device performance could be further improved, it should be noted that fundamental limitations to the device response arise from the equilibrium of the binding reaction and from mass-transport constraints.[9] Therefore, a more effective method to achieve higher-sensitivity detection on a rapid timescale is in great demand.

The electrokinetic manipulation of particles has particular application in biotechnology. Preconcentration by electrokinetics is an alternative approach for high-sensitivity protein detection, and it has many advantages,[10,11] such as shorter concentration time (usually within a few minutes), multiple tunable parameters, easy and flexible electrode design and fabrication, and feasible miniaturization and integration (e.g., significant reduction in operating voltage, electrical heating, and electrochemical effects). It is reported that the electrokinetic trapping of nanofluidic filter could increase the protein concentration by ≈6–8 orders of magnitude.[12] Choi et al. used dielectrophoresis (DEP) to concentrate single- and double-stranded DNA,[13] and the enrichment of $\approx 10^3$–10^5 was obtained for bacteria *Escherichia coli* concentration.[14] In most cases, particles are immobilized at a specific position and released by lowering the applied voltage. However, unwanted disturbance on FET electrical signals might be caused by the additional voltage tuning.

In order to push the detection limit with electrokinetic method while overcoming the possible adverse effect of

[*] Prof. J.-R. Gong
National Center for Nanoscience and Technology, China
Zhongguancun Beiyitiao No.11
Beijing 100190 (P. R. China)
E-mail: gongjr@nanoctr.cn

Supporting Information is available on the WWW under http://www.small-journal.com or from the author.

DOI: 10.1002/smll.200902132

changing electrokinetic parameters on signal measurements, the integrated nanoelectronic and electrokinetic device is developed and reported in this paper. NW devices modified with monocolonal antibody (mAb) for prostate specific antigen (PSA) are shown to exhibit $\approx 10^4$ increase in sensitivity with the excitation of an AC signal. The streaming DEP increases the protein concentration at the sensor surface and the induced electrostatic interaction enhances protein association after the electrokinetic application. Integrated NW devices are also modified with receptors for the detection of cholera toxin subunit B (CTB), and the results show general applicability of this method.

2. Results and Discussion

2.1. Overview of Approach

A schematic image depicting the integrated device used in the experiment is shown in Scheme 1a. An electrically addressable Si NWFET is defined at the micrometer-sized gap of the electrokinetic electrode pair by photolithography and metal deposition, and it is also displayed by a top-view field-emission scanning electron microscopy (FE-SEM) image in Scheme 1b. After putting the poly(dimethylsiloxane) (PDMS) with a channel on the functionalized chip for microfluidic sample delivery, an integrated NW sensor biochip was obtained. In a previous experiment,[5] only NWFET was used for protein detection, and there was no AC electrokinetic electrode. Thus, the protein concentration near the NW surface is almost the same as the injected concentration, as illustrated by the cross section of the flow channel in Scheme 1c. After the AC signal is applied, the AC electric field generated by coplanar microelectrodes produces a steady fluid flow pattern, moving out across the surface and dragging embedded analytes regardless of size down to the gap of electrodes in electrolytic solution, as shown in Scheme 1d.[15] The mechanism responsible for the flow is the interaction of the tangential component of the electric field and the induced charge in the diffuse double layer on the electrode surface, called AC electro-osmosis, which is independent of the sign of the electrode.[16]

However, AC electro-osmosis neither concentrates nor rarefies analytes. In a diverging field the polarized particles experience a force that can cause them to move to regions of high or low electric field, depending on the particle polarizability compared with the suspending medium. The motion produced by this force is called DEP. DEP force arising from the nonuniform AC electric field is responsible for the formation of protein enhancement and depletion regions in the flow channel.[17] Thus, concentrated streaming could be formed near the NW surface, corresponding to the enhanced sensing signal with the excitation of AC electric field. This combined mechanism, AC electro-osmosis for transport and DEP for concentration, is called streaming DEP here. There are several advantages to this mechanism. First, more analytes could be concentrated with smaller voltages due to the flow transport. Second, removal of the concentrate is quite easy and quick. Thus, continuous detection is possible without additional voltage tuning and the response time is significantly shortened when convective effects instead of diffusion become

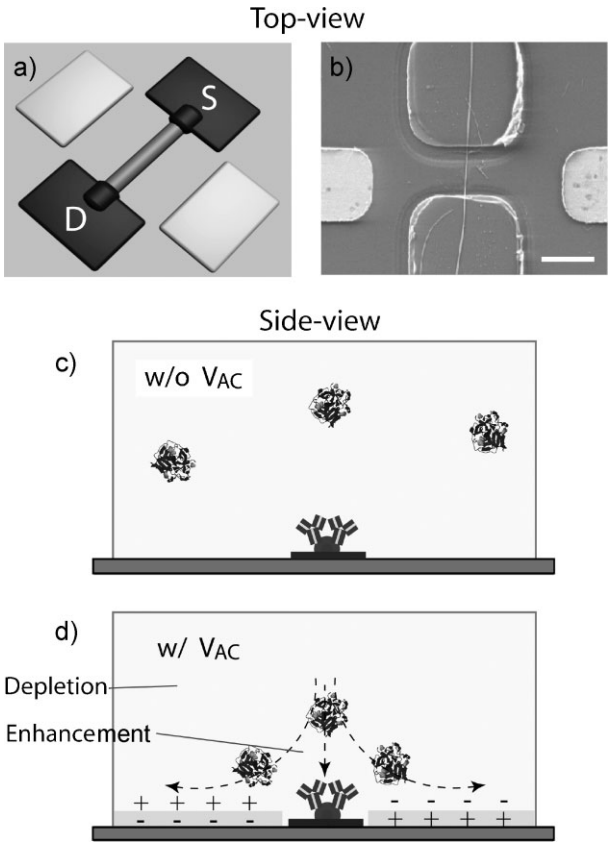

Scheme 1. a) Schematic image of the integrated nanoelectronic and electrokinetic device. The NW is contacted with two electrodes, source (S) and drain (D), for measuring conductance. A pair of parallel coplanar plate electrodes is added near the NW. b) Top-view field-emission SEM image of the integrated device. Scale bar is 2 μm. c) Schematic image of the microfluidic channel cross section showing the protein binding at the original injected concentration near the NW surface without AC excitation. d) Schematic image of the microfluidic channel cross section showing the protein binding at the enhanced concentration near the NW surface with AC excitation.

important.[9] Third, electrostatic interactions caused by the induced polarization charge under the applied electric field enhance the binding affinity because the favorable Coulomb interaction energy between the receptor and the analyte.[18] It is also found that electrostatics can enhance both affinity and specificity simultaneously.[19,20]

2.2 PSA Sensing Without and With AC Excitation

Cancer protein marker PSA was chosen as the initial target for these studies because of its importance in the detection of prostate and breast cancer, which are the most common cancers and an important cause of cancer death among American men and women, respectively.[21] The NW surface linkage chemistry for PSA detection is similar to the previous procedure (Figure 1a),[5] including conjugation of the mAbs with the aldehyde groups coupled to the Si NW surface, and subsequent block of unreacted free aldehyde groups to prevent nonspecific binding.

The sensitivity limit of the Si NW device without AC application was first determined by measuring conductance

NANO MICRO small

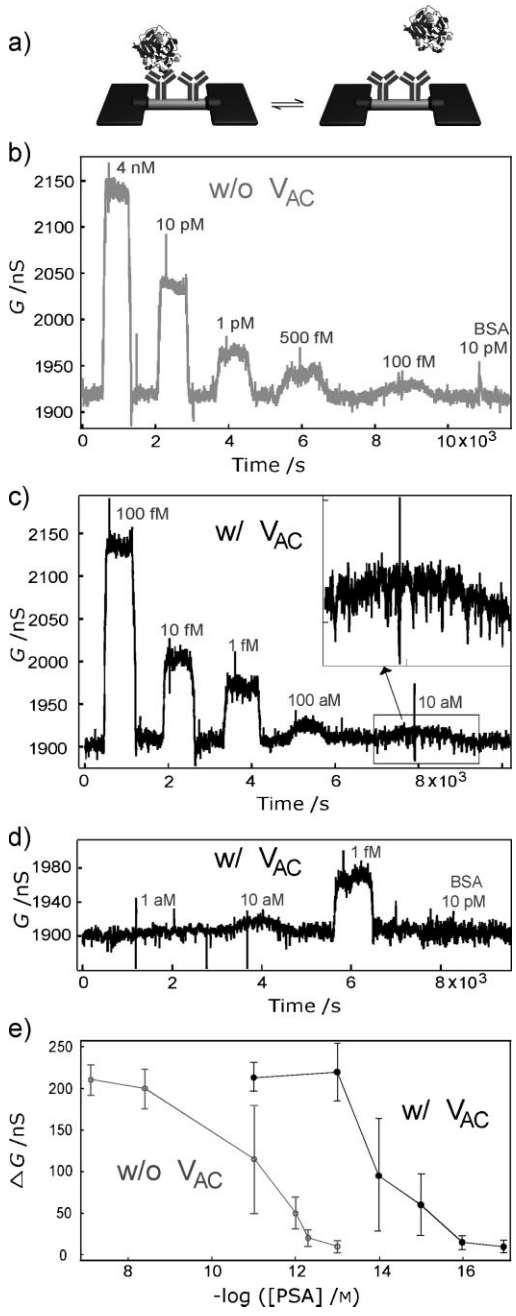

Figure 1. a) Schematic image of PSA binding and unbinding on Si NW sensor surface, where the PSA antibodies are coupled to the aldehyde groups through covalent interaction. b) Conductance-versus-time data recorded after alternate delivery of 10 μM phosphate buffer and the following protein solutions without AC excitation. The order of protein delivery: 1) 4 nM PSA, 2) 10 pM PSA, 3) 1 pM PSA, 4) 500 fM PSA, 5) 100 fM PSA, and 6) 10 pM BSA. Sharp spikes might be caused when switching the solutions but having little effect on sensing results. Source/drain modulation: a 3 Hz sine wave with a 30 mV amplitude at zero DC bias. c,d) Conductance-versus-time data recorded after alternate delivery of 10 μM phosphate buffer and various concentrations of protein solutions with AC excitation (0.5 V, 47 Hz). Source/drain modulation: a 79 Hz sine wave with a 30 mV amplitude at zero DC bias. c) The order of protein delivery: 1) 100 fM PSA, 2) 10 fM PSA, 3) 1 fM PSA, 4) 100 aM PSA, and 5) 10 aM PSA. Inset: Zoomed-in image of 10 aM PSA delivery. d) The order of protein delivery: 1) 1 aM PSA, 2) 10 aM PSA, 3) 1 fM PSA, 4) 10 pM BSA. e) Comparison of plots of conductance change versus concentration of PSA without and with AC excitation in 10 μM ionic strength phosphate buffer solution.

changes at various PSA concentrations as a control experiment. Representative time-dependent data (Figure 1b) showed a well-defined conductance increase and subsequent return to baseline when PSA solution and phosphate buffer were alternately delivered through the microfluidic channel to the device. The isoelectric point (pI) of PSA is 6.8,[22] so PSA binding to the p-type NW device causes the conductance increase at pH 7.4 in the experiments.[5] It could be seen that the conductance change was concentration dependent with the detection limit of 100 fM. No binding signal was observed when 10 pM bovine serum albumin (BSA) solution was delivered to the device, demonstrating good specificity of the sensor.

The data in Figure 1c show the conductance-versus-time measurements at different PSA concentrations when AC electric field (sine wave of 0.5 V, 47 Hz) was excited. The reproducibility and selectivity of the sensor were also investigated. Similar conductance changes were observed when 10 aM and 1 fM solutions of PSA were repeatedly delivered to the device. These results showed that reproducible device sensitivity was achieved. The delivery of a 10 pM BSA solution and 1 aM PSA, with AC excitation, caused little conductance change (Figure 1d), demonstrating excellent selectivity of the device, and meanwhile excluding the possible artifact caused by AC excitation. Sometimes, a little shift of the baseline of NW conductance, such as a ≈10 nS decrease of baseline, was observed when the AC signal was just started. It might be due to the change of the electrode static potential in solution but with little effect on the magnitude of sensing signals. Comparison of the plots of conductance change versus PSA concentration clearly shows the dramatic increase in sensitivity with AC application (Figure 1e). The sensing signal could reach saturation when 100 fM PSA was delivered to the device with AC excitation, whereas 4 nM PSA was needed to saturate the sensing signal without AC excitation. A $\approx 10^4$ increase in sensitivity was obtained by comparing the detection limit with and without AC excitation. The above sensorgrams are the average results on many devices, and the variation in the magnitude of sensing signals among different devices are shown by the error bar. The protein detection limit reported here is in the same order as that reported by nanoparticle,[23] and three orders of magnitude better than the best result from NW sensors reported by Zheng et al.[5] Note that 1) in the AC experiments, the potential is always on during the process of switch of protein and buffer and change of protein concentrations; 2) the real binding concentration is higher than the injected concentration at the NW surface after the electric-field application; the feasibility of the detection limit is analyzed in the Supporting Information.

2.3. Optimization of AC Electrokinetic Parameter

The enhancement effect of the integrated devices was measured as a function of the frequency, voltage, and solution ionic strength to optimize AC electrokinetic parameters, which also provides proof of the AC electrokinetic mechanism.

First, a series of tests to investigate the effect of frequency on sensing signal were performed by delivering 100 fM PSA in 10 μM phosphate buffer at a fixed 0.5 V voltage. AC electro-osmosis has an origin similar to DC electro-osmosis. For AC

voltages, double-layer polarization effects mean that the magnitude of tangential electric field $E_t(t)$ and surface charge density change $\Delta\sigma_q(t)$ will depend on frequency. The electrode–solution interface could be characterized by a double-layer capacitance. At high frequencies, the potential is dropped entirely across the electrolyte. Since $\Delta\sigma_q(t)$ tends to zero, AC electro-osmosis flow will stop. At low frequencies, the electric field in the medium tends to zero. The tangential field must be continuous, so $E_t(t)$ in the double layer is also zero, and the flow will cease. Therefore, the maximum velocity of AC electro-osmosis flow occurs at intermediate frequencies.[15] As expected, the observed signal enhancement effect tends to be a minimum at low- (23 Hz) and high-frequency (1 kHz) limits, and has a maximum at an intermediate frequency of 47 Hz, as illustrated by the normalized response of NW sensor (Figure 2a) and the corresponding diagram of conductance change versus frequency (Figure 2b, •). The result is consistent with the reported frequency-dependent AC electrokinetic phenomenon.[15] It indicates that the electrokinetic phenomenon is responsible for the observed enhancement effect. This frequency-dependent relationship also excludes electrothermal effects, which are independent of frequency except around charge relaxation frequency.[16]

Next, the effect of AC voltage on sensing signal was investigated at the same PSA concentration as used in the previous step at fixed 47 Hz. Enhanced binding signals were observed with the increase of the magnitude of AC voltage from 0.1 V to 0.5 V, as illustrated by the normalized sensorgrams (Figure 2c,) and the corresponding diagram of conductance change versus voltage (Figure 2d, •). As reported, higher voltage could cause more obvious electrokinetic phenomenon.[10,24] Due to the concern of the possible adverse effect of higher voltage on the device stability, 0.5 V was the maximum value used for sensing.

Last, the effect of solution ionic strength on sensing signal was studied. The optimal frequency at 10 pM PSA concentration in 1 mM buffer shifts to a higher frequency of 200 Hz compared to that in lower-ionic-strength solution (Figure 2b, ×), which is in agreement with the AC electrokinetic phenomenon that the frequency maximum increases with the increase of medium conductivity.[24] An increase of voltage also has a similar effect to that described in lower-ionic-strength buffer (Figure 2d, ×). An AC signal of 0.5 V, 200 Hz combining with the FET source/drain modulation (30 mV, 79 Hz) was chosen as the optimal operation parameter for sensing in 1 mM buffer. Under the optimal parameter, the detection limit of PSA is 2 fM with AC excitation (Figure 2f) compared to 10 pM without AC excitation (Figure 2e) in 1 mM buffer, with a 5000-fold increase in sensitivity. The enhancement order is less than that in the lower ionic buffer because the rate of electrokinetic flow is much lower in higher ionic solution due to the solution ionic strength dependent electrokinetic characteristic, corresponding to the less electrokinetic enhancement. Electrolyte-concentration-dependent Debye screening also makes the signal detection more difficult in higher ionic solution.[24]

An AC signal of 0.5 V, 47 Hz applied on the electrokinetic electrode combining with the FET source/drain modulation (30 mV, 79 Hz) in 10 μM ionic strength buffer was chosen as the optimal operation parameter for measuring the detection limit

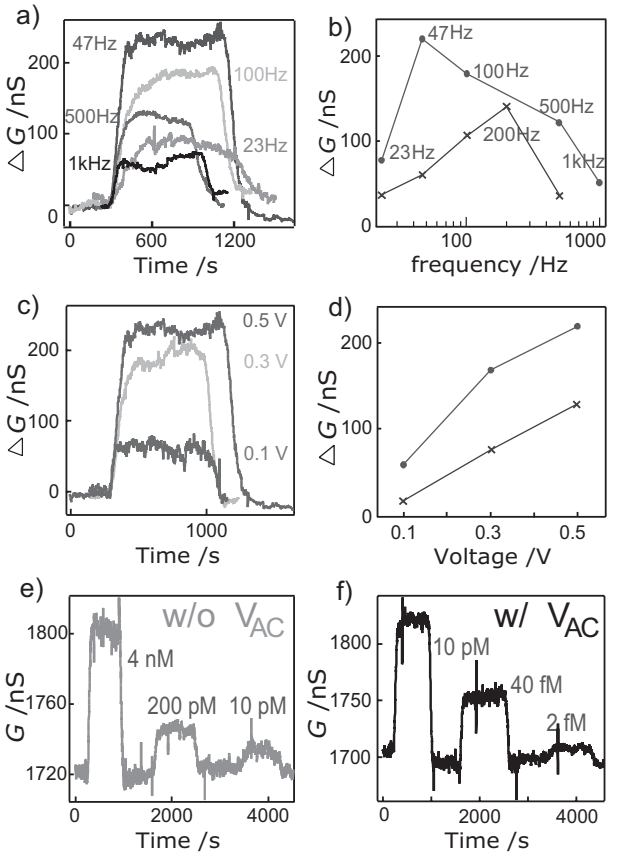

Figure 2. Optimization of AC electrokinetic parameters. a) Normalized overlay of conductance-versus-time data recorded by delivering 100 fM PSA at a fixed 0.5 V voltage with various frequencies in 10 μM ionic strength buffer solution. Source/drain modulation: a 79 Hz sine wave with a 30 mV amplitude at zero DC bias. b) AC frequency-dependent conductance change at 0.5 V (•: in 10 μM phosphate buffer, 100 fM PSA; ×: in 1 mM phosphate buffer, 10 pM PSA). c) Normalized overlay of conductance-versus-time data recorded by delivering 100 fM PSA at fixed 47 Hz AC frequency with various voltages in 10 μM ionic strength phosphate buffer solution. Source/drain modulation: a 79 Hz sine wave with a 30 mV amplitude at zero DC bias. d) AC voltage-dependent conductance change (•: in 10 μM phosphate buffer, 100 fM PSA, 47 Hz AC signal; ×: in 1 mM phosphate buffer, 10 pM PSA, 200 Hz AC signal). e) Conductance-versus-time data recorded after alternate delivery of 1 mM phosphate buffer and the following PSA solutions without AC excitation. The order of PSA delivery: 1) 4 nM, 2) 200 pM, and 3) 10 pM. Source/drain modulation: a 3 Hz sine wave with a 30 mV amplitude at zero DC bias. f) Conductance-versus-time data recorded after alternate delivery of 1 mM phosphate buffer and the following PSA solutions with AC excitation (0.5 V, 200 Hz). The order of PSA delivery: 1) 10 pM, 2) 40 fM, and 3) 2 fM. Source/drain modulation: a 79 Hz sine wave with a 30 mV amplitude at zero DC bias.

of the integrated device. The enhancement effect of the integrated device is dependent on electrokinetic parameters, such as frequency, voltage, and solution ionic strength, demonstrating that the AC electrokinetic mechanism plays a dominant role in improving device sensitivity in the experiment.

2.4. General Applicability

The above results using antibody-functionalized devices demonstrate high selectivity and sensitivity for protein

NANO MICRO small

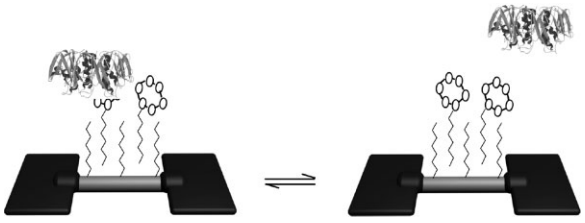

Scheme 2. Schematic image of CTB binding and unbinding on Si NW sensor surface, where the hydrocarbon chains of gangliosides are inserted into the silane monolayer via hydrophobic interaction.

detection. If the devices are modified with receptors other than antibodies, such as cellular receptors, more research areas could be explored to extend the application potential of the NW sensor. Gangliosides are abundant in cell membranes,[25] and Si NW devices modified with gangliosides could provide an analog to the outer lipid layer of membranes for detecting the binding affinity and specificity of proteins. Immobilization procedures are different from those used for antibodies: the hydrocarbon chains of gangliosides are inserted into the dodecyldimethylcholorosilane (DMCS) monolayer on NW surface via hydrophobic interactions, exposing the sugar receptor sites to the solution, as illustrated in Scheme 2.[26]

CTB is positively charged (pI is ≈7.5) in the buffer solution (pH = 6.7),[27] so the conductance-versus-time data recorded from p-type NW after introduction of CTB show a conductance decrease followed by a return to the conductance baseline value of the device after introduction of the buffer solution. CTB was used as the binding toxin due to its higher affinity for ganglioside GM1.[28] The magnitudes of the conductance change were concentration dependent and with a detection limit of 180 fM without AC excitation, as shown in Figure 3a. When an AC electric field was applied, a similar detection limit to PSA was obtained for CTB binding on ganglioside. The same magnitudes of binding signal as before after repetitive injections of 18 aM and 180 aM CTB solutions, respectively, shown in Figure 3b, demonstrate the device's good reproducibility. It is also observed that the magnitude of the noise is very small. The noise in the sensing experiment comes from a few sources, such as the disturbance of electric/magnetic fields and mechanic noises from the operating environment and the operator, the current leakage between the device and solution, and the intrinsic noise due to the transport of carrier in the device; the level of the noise might vary between different experiments. For the two detection systems, the main difference is the surface modification method, that is, antibody and cell-receptor modification; the latter can form a dense monolayer on the NW surface instead of the relatively loose multilayer by the former, which greatly decreases the level of noise and improves the stability of the signal. The high-sensitivity detection of the CTB versus ganglioside binding with AC excitation indicates the potential availability of the integrated device in various sensing systems.

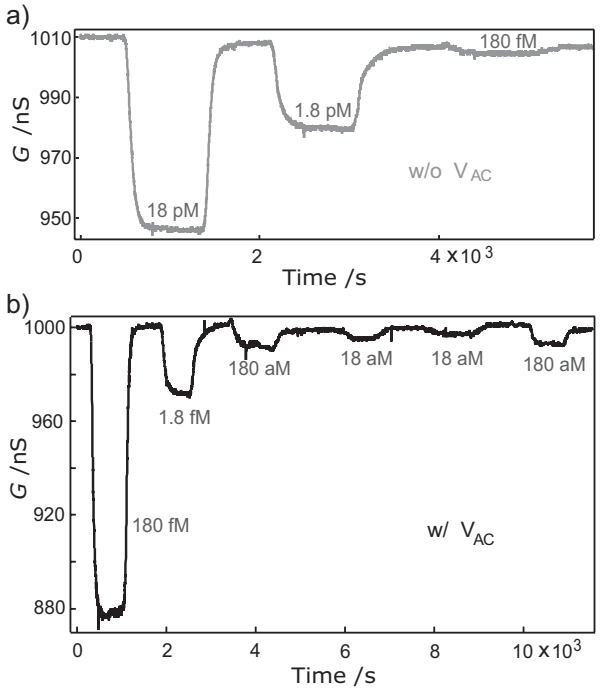

Figure 3. Real-time detection of CTB binding. a) Conductance-versus-time data recorded after alternate delivery of buffer and the following CTB solutions without AC excitation. The order of CTB delivery: 1) 18 pM, 2) 1.8 pM, and 3) 180 fM. Source/drain modulation: a 3 Hz sine wave with a 30 mV amplitude at zero DC bias. b) Conductance-versus-time data recorded after alternate delivery of phosphate buffer and the following CTB solutions with AC excitation (0.5 V, 47 Hz). The order of CTB delivery: 1) 180 fM, 2) 1.8 fM, 3) 180 aM, 4) 18 aM, 5) 18 aM, and 6) 180 aM. Source/drain modulation: a 79 Hz sine wave with a 30 mV amplitude at zero DC bias.

2.5. Discussion

When DEP is combined with electro-osmosis, three typical cases exist. At low electric field, DEP can be neglected and the electro-osmotic flow does not concentrate proteins. Above the DEP trapping threshold, proteins can be immobilized. At the intermediate conditions, DEP is unable to immobilize proteins against the electro-osmotic conveyance, and proteins will concentrate and rarefy into flowing filamentary streams, as shown in Scheme 1d.[29] Quantitative electric-field simulation, shown in Figure 4, shows that the applied electric-field strength near the sensor in the experiment is on the order of 10^5 V m^{-1} and with a field gradient 10^{11} V m^{-2}, which is not enough to trap protein molecules but is high enough to form the concentrated protein streaming compared with that reported in the literature.[13,29] Besides the concentration effect due to the formation of concentrated streamline between the AC electrokinetic electrode pair, the same phenomenon could be formed with less effect between the source and drain electrode due to AC modulation on FET. Similar particle aggregation due to hydrodynamic effects at the center gap region of four electrodes was reported.[11]

Although favorable intramolecular electrostatic interactions are frequently observed within individual binding partners, their role in enhancing molecular association has not been generally appreciated. A complementary shape or charge distribution is needed for a ligand to bind to the target receptor, and van der Waals and electrostatic interactions across the binding interface are driving forces forming the complex. The addition of partial charges to the receptor and

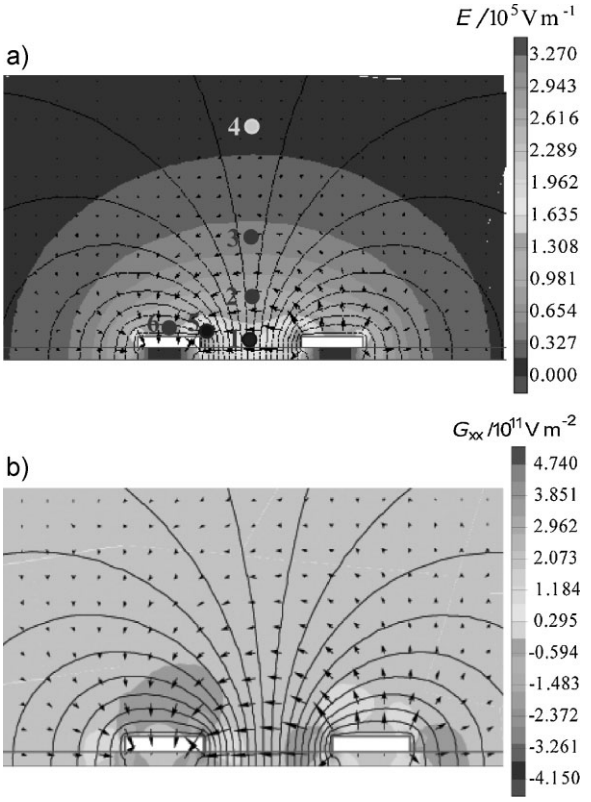

Figure 4. a) Field strength and b) field gradient near the electrokinetic electrodes from two-dimensional electrostatic simulations. Positions of the electric field measurement in (a): 1) $X = 0$, $Y = 0$ (in the middle of the electrode pair gap on the substrate; 2) $X = 0$, $Y = 2.5$ μm; 3) $X = 0$, $Y = 5$ μm; 4) $X = 0$, $Y = 10$ μm; 5) electrode edge; 6) electrode center. The order of field strength at the specific position: $5 > 1 > 6 > 2 > 3 > 4$ (see color images in Figure S2 of Supporting Information for clarity).

analyte after applying the electric field results in a favorable binding free energy.[19] Besides the optimal receptor–analyte electrostatic binding free energy, many suboptimal charge distributions also have favorable binding affinity, that is, the unbound analyte interacts with other receptor charges in close proximity and bound-state receptor interactions with the neighbors of its direct partner. Groups of same-signed charge increase the binding affinity over arrangements in which charges alternate sign in a local region of the receptor due to the stronger charge effect. Many charges decorate the binding site on the NW surface and same-signed charges or aligned oriented dipoles are in close proximity after the application of the electric field, providing an excellent interface for obtaining very favorable electrostatic binding.[20] Furthermore, the circular flow caused by electrokinetics is perpendicular to the original flow direction in the PDMS channel and increases the amount of time that analytes stay close to receptors, allowing sufficient opportunity for receptors to rotate into a proper orientation for binding and creating more productive collisions referring to the single collision dealt with in reaction due to diffusion in the flow channel.[30]

The reaction between proteins and surface receptors can be regarded as a simple reaction: $P + S \leftrightarrow P\bullet S$, where P, S, and P•S stand for free protein, immobilized surface receptor, and protein–receptor complex, respectively, and is assumed to follow pseudo first-order reaction kinetics. If assuming the magnitude of the SiNW sensor conductance signal (ΔG) is directly proportional to the concentration of protein–receptor complex, [P•S], the binding curve should have a single exponential shape, that is, $\Delta G \propto A \times \exp(-k_{obs} \times t)$, where A is the signal magnitude, k_{obs} represents the observed kinetic rate constant of this reaction, and t is the rising time. Analysis of the binding/unbinding curve was performed (an illustration from 1.8 fM CTB sensing is shown in Figure S1 of the Supporting Information, showing the conductance signal versus time traces with an expanded x-scale), and the single exponential fitting is used to extract the kinetics information. Based on the theoretical equation, k_{obs} is linear to the CTB concentration for the binding phase, that is, $k_{obs} = k_{on} \times C + k_{off}$, where C stands for the protein concentration, and k_{on} and k_{off} represent the association and disassociation rate constants ($K_d = k_{off}/k_{on}$), respectively.[31,32] To get a rough idea of binding/unbinding kinetics with the AC application, the equilibrium disassociation constant K_d (1.2 nM) of GM1 and CTB[33] without AC application obtained from the same method as abovementioned is taken as a given quantity since the concentrated protein concentration near the sensor surface is unknown. Therefore, k_{on} and k_{off} are obtained as 6.8×10^6 M^{-1} S^{-1} and 8.2×10^3 S^{-1}, respectively, which are similar to the values in the case without AC application.[33] However, it can be clearly observed that the rising time decreases (faster binding occurs) with AC application compared to that without AC application at the same injected protein concentration due to the increased protein concentration near the sensor surface with AC. If the binding affinity (association constant $K_a = 1/K_d$) increases then k_{on} will probably increase.

Specific advances have been made with other label-free detection approaches, including nanotube sensors,[34] surface plasmon resonance (SPR),[35] microcantilevers,[36] and quartz-crystal microbalance.[37] While the highest sensitivity reported for the detection of proteins is obtained by nanoparticle labeling assay with the PCR application,[38] it is not suitable for real-time detection and kinetic analysis.

3. Conclusions

In summary, NW devices modified with antibody for PSA exhibit up to a 10^4 increase in sensitivity due to streaming dielectrophoresis and corresponding electrostatic contribution to the binding affinity after AC electric-field application. The devices are also modified with receptors for CTB, and results show general applicability of this method. These studies demonstrate that the integrated nanoelectronic and electrokinetic device is developed for attomolar protein detection, and should open opportunities in early stage disease detection and the analysis of proteins from single cells.

4. Experimental Section

Integrated nanoelectronic and electrokinetic device fabrication: Chemical vapor deposition was used for Si NW synthesis.[39] In this method, an atomic ratio of 1:4000 diborane was doped into

NANO MICRO small

reactant silane with 20-nm gold nanoclusters as catalysts. Si NW devices were defined using photolithography with Ni metal contacts and subsequent 60-nm-thick Si_3N_4 coating of Ni on a 600-nm thermal oxide Si substrates. The coplanar plate electrokinetic electrodes consist of 1-nm titanium, 50-nm gold, and 15-nm titanium.

NW surface modification with antibody: Linking antibody receptors to the surfaces of the Si NW followed the previous procedure.[5] First, the devices are dipped in a 1% ethanol solution of 3-(trimethoxysilyl)propyl aldehyde (United Chemical Technologies, Bristol, PA) for ≈20 min, then rinsed with ethanol, and cured for 10 min at 110 °C. After that, the mAb, anti-PSA (AbI, clone ER-PR8, NeoMarkers) is coupled to the aldehyde-terminated NW surfaces by reaction of antibody (10–100 μg mL^{-1}) in a pH 8.4, phosphate buffer solution (10 mM) with the a sodium cyanoborohydride catalyst (4 mM) for a period of 2–3 h. Last, the unreacted aldehyde surface groups are blocked with ethanolamine under similar solution conditions as used for Ab modification for a period of 1–2 h.

NW surface modification with ganglioside: First, the NW devices are incubated in 2% dodecyldimethylcholorosilane (Sigma Inc.) anhydrous toluene solution with N_2 protection for 8–16 h. Then, the chip is baked at 120 °C for 15 min followed by rinsing with anhydrous toluene and ethanol. After that, the solution of monosialoganglisides (Sigma Inc.) with concentration 0.1–1 μg mL^{-1}) is deposited in the phosphate buffer (0.1 M, pH 8.4) onto the NW surface for a period of 4 h.

Protein samples: PSA, CTB, and BSA were used without further purification on receipt from Calbiochem, and diluted in the phosphate buffer prior to sensing measurements as described before.[5]

Electrical Measurements: A DSP dual-phase lock-in amplifier (Stanford Research Systems Inc.) and a current pre-amplifier (DL Instrument Inc., Model 1211) were used to continuously record the conductance versus time data when different protein solutions and phosphate buffer were alternately delivered into the microfluidic channel. The 30 mV lock-in parameter sets the zero DC source/drain potential to avoid electrochemical reactions. The AC signal for the electrokinetic application was provided by a function generator (Agilent 33220A, 20 MHz).

Acknowledgements

J.-R.G. sincerely thanks Prof. Charles M. Lieber at Harvard University for his support and Dr. Gengfeng Zheng for helpful discussion. Financial support from the National Basic Research Program of China (973 Program, No. 2009CB930200), Special Presidential Foundation of Chinese Academy of Sciences (No. 09312911ZX), and Special National Natural Science Foundation of China (No. Y0191111JJ) is gratefully acknowledged.

[1] R. Etzioni, N. Urban, S. Ramsey, M. McIntosh, S. Schwartz, B. Reid, J. Radich, G. Anderson, L. Hartwell, *Nat. Rev. Cancer* **2003**, *3*, 1.
[2] D. M. Bravata, K. M. McDonald, W. M. Smith, C. Rydzak, H. Szeto, D. L. Buckeridge, C. Haberland, D. K. Owens, *Ann. Intern. Med.* **2004**, *140*, 910.
[3] G. S. Makowski, E. L. Davis, S. M. Hopfer, *Ann. Clin. Lab. Sci.* **1996**, *26*, 458.
[4] F. Patolsky, G. Zheng, C. M. Lieber, *Nanomedicine* **2006**, *1*, 51.
[5] G. Zheng, F. Patolsky, Y. Cui, W. U. Wang, C. M. Lieber, *Nat. Biotechnol.* **2005**, *23*, 1294.
[6] J. Hahm, C. M. Lieber, *Nano Lett.* **2004**, *4*, 51.
[7] F. Patolsky, G. Zheng, O. Hayden, M. Lakadamyali, X. Zhuang, C. M. Lieber, *Proc. Natl. Acad. Sci. USA* **2004**, *101*, 14017.
[8] E. Stern, J. F. Klemic, D. A. Routenberg, P. N. Wyrembak, D. B. Turner-Evans, A. D. Hamilton, D. A. LaVan, T. M. Fahmy, M. A. Reed, *Nature* **2007**, *445*, 519.
[9] M. J. Eddowes, *Biosensors* **1987/88**, *3*, 1.
[10] E. B. Cummings, A. K. Singh, *Anal. Chem.* **2003**, *75*, 4724.
[11] M. P. Hughes, H. Morgan, F. J. Rixon, J. P. H. Burt, R. Pethig, *Biochim. Biophys. Acta* **1998**, *1425*, 119.
[12] Y.-C. Wang, A. L. Stevens, J. Han, *Anal. Chem.* **2005**, *77*, 4293.
[13] C.-F. Chou, J. O. Tegenfeldt, O. Bakajin, S. S. Chan, E. C. Cox, N. Darnton, T. Duke, R. H. Austin, *Biophys. J.* **2002**, *83*, 2170.
[14] C.-F. Chou, F. Zenhausern, *IEEE Eng. Med. Biol. Mag.* **2003**, *22*, 62.
[15] A. Ramos, H. Morgan, N. G. Green, A. Castellanos, *J. Colloid Interface Sci.* **1999**, *217*, 420.
[16] A. Ramos, H. Morgan, N. G. Green, A. Castellanos, *J. Phys. D: Appl. Phys.* **1998**, *31*, 2338.
[17] N. G. Green, A. Ramos, A. Gonzáles, H. Morgan, A. Castellanos, *Phys. Rev. E* **2002**, *66*, 026305-1.
[18] L. Y. Zhang, E. Gallicchio, R. A. Friesner, R. M. Levy, *J. Comput. Chem.* **2001**, *22*, 591.
[19] E. Kangas, B. Tidor, *J. Chem. Phys.* **1998**, *109*, 7522.
[20] L. T. Chong, S. E. Dempster, Z. S. Hendsch, L.-P. Lee, B. Tidor, *Protein Sci* **1998**, *7*, 206.
[21] A. Jemal, R. Siegel, E. Ward, T. Murray, J. Xu, M. J. Thun, *CA Cancer J. Clin.* **2007**, *57*, 43.
[22] D. A. Armbruster, *Clin. Chem.* **1993**, *39*, 181.
[23] J.-M. Nam, C. S. Thaxton, C. A. Mirkin, *Science* **2003**, *301*, 1884.
[24] P. K. Wong, C.-Y. Chen, T.-H. Wang, C.-M. Ho, *Anal. Chem.* **2004**, *76*, 6908.
[25] S. Kozaki, Y. Kamata, T. Nishiki, H. Kakinuma, H. Maruyama, H. Takahashi, T. Karasawa, K. Yamakawa, S. Nakamura, *Infect. Immun.* **1998**, *66*, 4811.
[26] a) Y. Fang, A. G. Frutos, J. Lahiri, *Langmuir* **2003**, *19*, 1500; b) C. R. MacKenzie, T. Hirama, K. K. Lee, E. Altman, N. M. Young, *J. Biol. Chem.* **1997**, *272*, 5533; c) A. Janshoff, C. Steinem, M. Sieber, A. el Bayâ, M. A. Schmidt, H. J. Galla, *Eur. Biophys. J.* **1997**, *26*, 261.
[27] J. J. Mekalanos, *Methods Enzymol.* **1988**, *165*, 169.
[28] M. A. Cooper, *J. Mol. Recognit.* **2004**, *17*, 286.
[29] E. B. Cummings, *IEEE Eng. Med. Biol. Mag.* **2003**, *22*, 75.
[30] F. B. Sheinerman, R. Norel, B. Honig, *Curr. Opin. Struct. Biol.* **2000**, *10*, 153.
[31] R. Karlsson, A. Michaelsson, L. Mattsson, *J. Immunol. Methods* **1991**, *145*, 229.
[32] D. G. Myszka, *Curr. Opin. Biotech.* **1997**, *8*, 50.
[33] G. Zheng, Ph. D. Thesis, Harvard University, USA 2006.
[34] Z. Liu, S. M. Tabakman, Z. Chen, H. Dai, *Nat. Protoc.* **2009**, *4*, 1372.
[35] X. D. Hoa, A. G. Kirk, M. Tabrizian, *Biosens. Bioelectron.* **2007**, *23*, 151.
[36] S. K. Vashist, *J. Nanotechnol. Online* **2007**, *3*, 1.
[37] E. R. Hirst, Y. J. Yuan, W. L. Xu, J. E. Bronlund, *Biosens. Bioelectron.* **2008**, *23*, 1759.
[38] T. Asefa, C. T. Duncan, K. K. Sharma, *Analyst* **2009**, *134*, 1980.
[39] Y. Cui, Z. Zhong, D. Wang, W. U. Wang, C. M. Lieber, *Nano Lett.* **2003**, *3*, 149.

Received: November 12, 2009
Revised: January 15, 2010
Published online: March 8, 2010

Submitted to small

Small

Label-free Attomolar Detection of Proteins Using Integrated Nanoelectronic and Electrokinetic Devices

*Jian Ru Gong**

National Center for Nanoscience and Technology, China
gongjr@nanoctr.cn
http://www.nanoctr.cn/gongjianru

Supporting Information

A roughly calculation, regarding the geometry of the sample cell and the flow regime operative in the experiment, was made to estimate the feasibility of the protein detection limit.

1. Antibody binding sites on NW surface

First, derive an approximate value for Γ_{lim} (represents the density of binding sites on the NW surface). Assuming that the protein comprising the surface immobilized binding site is roughly globular with a value for the radius, $r_0 \sim 2\times10^{-9}$ m, for close packing of spheres the site density (Γ_{lim})[1] is simply $1/2\sqrt{3}\,N_A r_0^2$ (N_A: Avogadro constant) M m^{-2} giving $\Gamma_{lim} \sim 1.125\times10^{-7}$ M m^{-2}.

$\Gamma_{lim} = 1.125\times10^{-7}\ \text{M m}^{-2} \times 6.02 \times 10^{23}\ \text{M}^{-1} \approx 7\times10^{16}\ \text{m}^{-2}$

Then, calculate the average surface area of NW ($\mathbf{S}_{NW}$), length of NW (L) is *ca.* 3 μm, radius of NW (r), 20 nm.

$\mathbf{S}_{NW} = 2\pi rL = 2 \times 3.14 \times 20 \times 10^{-9}\ \text{m} \times 3 \times 10^{-6}\ \text{m} \approx 3.8 \times 10^{-13}\ \text{m}^2$

Last, get antibody binding sites on NW surface (**N**)

$\mathbf{N} = \Gamma_{lim} \times \mathbf{S}_{NW} = 7 \times 10^{16}\ \text{m}^{-2} \times 3.8 \times 10^{-13}\ \text{m}^2 \approx 2.7 \times 10^4$

2. Feasible detection limit

From equilibrium considerations, the following expression in Equation (1) forms a useful basis to assess the likely performance of immunosensors, although its application to the description of antigen binding at surfaces will be subject to the well-known limitations of the Langmuir treatment.

$$1/\theta_{eq} = 1 + K/[A]_{eq} \quad (1)$$

Where, θ_{eq} is equilibrium surface coverage, as a function of normalized concentration, [A]/*K*. In our case, the equilibrium dissociation constant of PSA antibody and antigen, *K*, is *ca.* 0.2 nM;[2] PSA detection limit without AC electrokinetic application, $[A]_{eq}$ is 100 fM; Based on equation (1), θ_{eq} ~ 1/2000. At this low fractional surface coverage, that is, *ca.* 14 (**N**θ_{eq} = 2.7 $\times 10^4$ / 2000 = 14) antibody binding sites on NW surface, 100 fM detection limit should be feasible.

From kinetic considerations, two cases will serve to illustrate the important features of the surface binding reaction. The first is linear diffusion, and the second is the "Nernst diffusion layer" treatment of convective systems.

In the case of without AC excitation, the protein-NW collision/binding frequency (*J*) is estimated in Equation (2).

$$J = k\,[PSA] \quad (2)$$

Assuming the binding is diffusion limited, based on Fick's law, the number of molecules entering collision cross-section (cylinder shape) per unit time (rate)

$J = 2\pi r\, L\Phi_B = 2\pi r\, L\, D_B\, d[B]_r/dr$

Surface flux $\Phi_r(r) = -D_B \nabla C_B = -D_B\, d[B]_r/dr$

$$\int_{[B]_{R^*}}^{[B]} d[B]_r = \int_{R^*}^{d} \frac{J}{2\pi r L D_B} dr$$

$$[B]-[B]_{R^*} = [B] = \frac{J}{2\pi L D_B} \ln[r]_{R^*}^{d}$$

L, the length of NW; D_B, the diffusion coefficient, for most of proteins for similar size to PSA, ~10^{-10} m^2 s^{-1}; R^*, the radius of cross-section of interaction (wire+receptor); *d*, the distance where protein concentration equals to bulk, *i.e.*, wire+receptor+protein

$$k = \frac{J}{[B]} = \frac{2\pi L D_B}{\ln \frac{d}{R^*}}$$

So, for *d* = 30 nm, R^* = 25 nm, *L* = 3 μm, D_B = 10^{-10} m^2 s^{-1}, the encountering rate k = 6.3 $\times 10^{12}$ (M^{-1} s^{-1})

Through the comparison of the PSA-NW encounter rate and signal rising time in Table 1, it is feasible to have a number of binding events occurring at the lowest concentration (100 fM) without AC excitation in our experiment.

Table 1. PSA-NW encounter rate and event without electrokinetic application

[PSA] [pM]	PSA-NW encounter rate [s^{-1}][a]	Time for one event of PSA-NW encounter [s][a]	Signal rising time[s][b]	Possible encounter event during rising [b]
1	6.3	0.16	115	725
0.5	3.15	0.32	220	693
0.1	0.63	1.6	550	347

[a] Calculation result; [b] Experimental result.

When 10 aM PSA is delivered into the channel,

$$10 \times 10^{-18}\ \text{M} \times 6.02 \times 10^{23}\ \text{M}^{-1} = 6.02 \times 10^{3}\ \text{mL}^{-1}$$

at the delivery rate of 0.3 mL h^{-1},

$$0.3\ \text{mL h}^{-1} \times 6.02 \times 10^{3}\ \text{mL}^{-1} = 30\ \text{min}^{-1}$$

the number of molecule passing through the channel during the binding time of 600 s is,

$$30\ \text{min}^{-1} \times 600\ \text{s} = 300$$

Considering other possible negative effect, such as molecular adsorption in the channel, we conservatively assume that only 10% molecules could bind onto the NW after electrokinetic application, even so, still could get 30 molecules bound on the NW. Therefore, with the enrichment factor of 10^4, femtomolar protein concentration at the nanowire surface could be reached with the 10 aM injected concentration. Based on the calculation about diffusion model for femtomolar concentration without AC excitation, the detection limit of 10 aM with AC excitation is feasible.

References

[1] M. J. Eddowes, *Biosensors* **1987/88**, *3*, 1.

[2] T. Soukka, J. Paukkunen, H. Harma, S. Lonnberg, H. Lindroos, T. Lovgren, *Clin. Chem.* **2001**, *47*, 1269.

Color Schemes/Figures

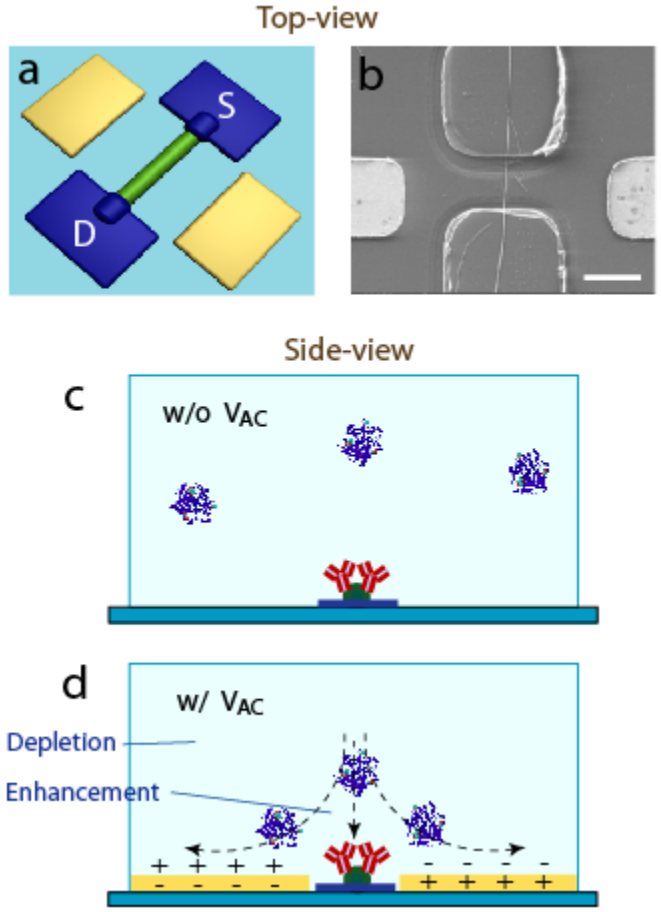

Scheme 1. a) Schematic of the integrated nanoelectronic and electrokinetic device. The NW is contacted with two electrodes, source (S) and drain (D), for measuring conductance. A pair of parallel coplanar plate electrodes is added near the NW. b) Top-view field-emission scanning electron image of the integrated device. Scale bar is 2 μm. c) Schematic of the microfluidic channel cross-section showing the protein binding at the original injected concentration near the NW surface without AC excitation. d) Schematic of the microfluidic channel cross-section showing the protein binding at the enhanced concentration near the NW surface with AC excitation.

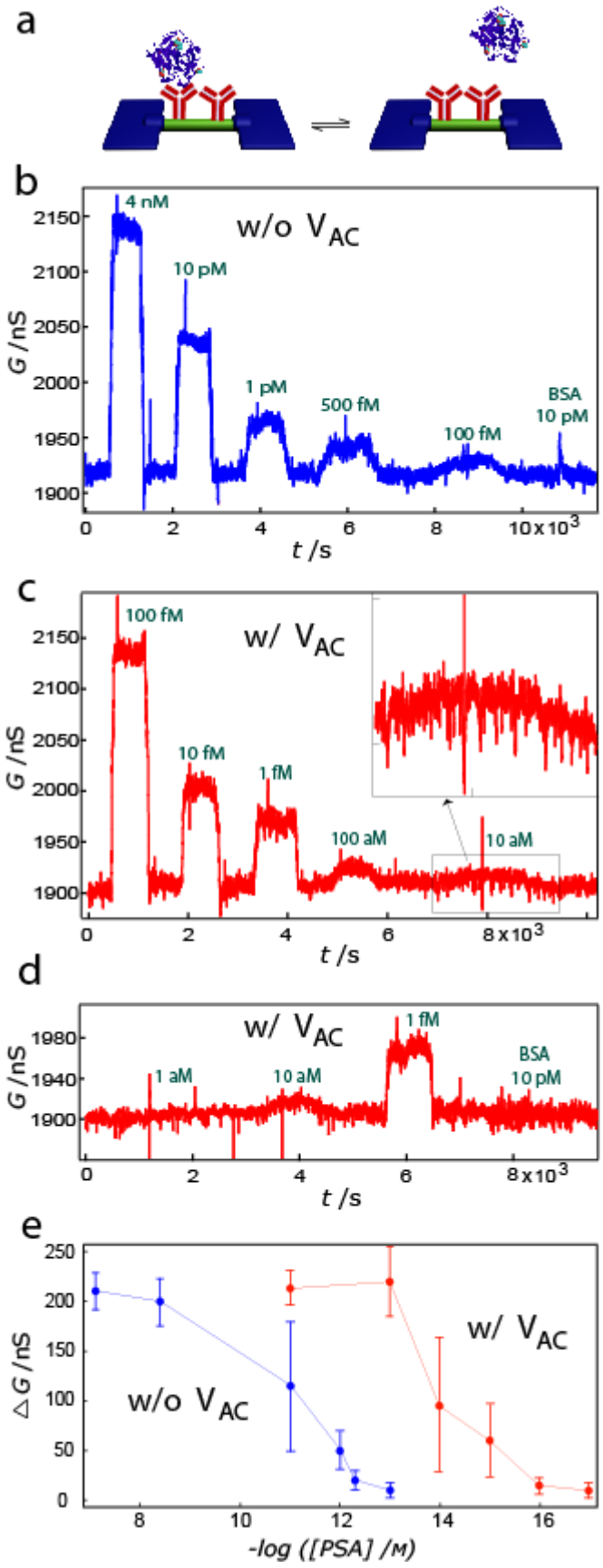

Figure 1. a) Schematic of PSA binding and unbinding on Si NW sensor surface, where the PSA antibodies are coupled to the aldehyde groups through covalent interaction. b) Conductance-versus-time data recorded after alternate delivery of 10 μM phosphate buffer and the following protein solutions without AC excitation. The order of protein delivery: (1) 4 nM PSA, (2) 10 pM PSA, (3) 1 pM PSA, (4) 500 fM PSA, (5) 100 fM PSA and (6) 10 pM BSA. Sharp spikes might be caused when switching the solutions, but having little effect on sensing results. Source/drain modulation: a 3 Hz sine wave with a 30 mV amplitude at zero DC bias. c,d) Conductance-versus-time data recorded after alternate delivery of 10 μM phosphate buffer and various concentrations of protein solutions with AC excitation (0.5 V, 47 Hz). Source/drain modulation: a 79 Hz sine wave with a 30 mV amplitude at zero DC bias. (c) The order of protein delivery: (1) 100 fM PSA, (2) 10 fM PSA, (3) 1 fM PSA, (4) 100 aM PSA and (5) 10 aM PSA. Inset: Zoomed-in image for 10 aM PSA delivery. (d) The order of protein delivery: (1) 1 aM PSA, (2) 10 aM PSA, (3) 1 fM PSA, (4) 10 pM BSA. e) Comparison of plots of conductance change versus concentration of PSA without and with AC excitation in 10 μM ionic strength phosphate buffer solution.

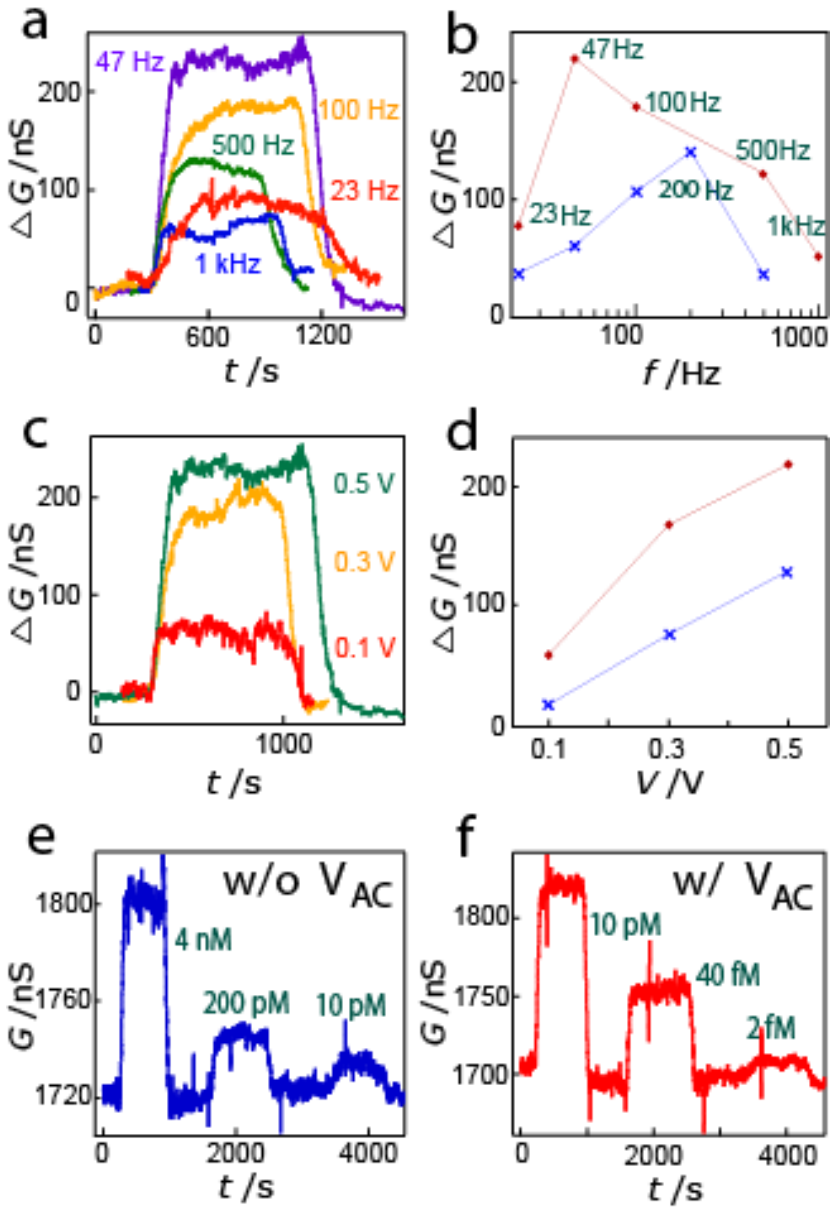

Figure 2. Optimization of AC electrokinetic parameters. a) Normalized overlay of conductance-versus-time data recorded by delivering 100 fM PSA at a fixed 0.5 V voltage with various frequencies in 10 μM ionic strength buffer solution. Source/drain modulation: a 79 Hz sine wave with a 30 mV amplitude at zero DC bias. b) AC frequency dependent conductance change at 0.5 V (●: in 10 μM phosphate buffer, 100 fM PSA; ×: in 1 mM phosphate buffer, 10 pM PSA). c) Normalized overlay of conductance-versus-time data recorded by delivering 100 fM PSA at fixed 47 Hz AC frequency with various voltages in 10 μM ionic strength phosphate buffer solution. Source/drain modulation: a 79 Hz sine wave with a 30 mV amplitude at zero DC bias. d) AC voltage dependent conductance change (●: in 10 μM phosphate buffer, 100 fM PSA, 47 Hz AC signal; ×: in 1 mM phosphate buffer, 10 pM PSA, 200 Hz AC signal). e) Conductance-versus-time data recorded after alternate delivery of 1 mM phosphate buffer and the following PSA solutions without AC excitation. The order of PSA delivery: (1) 4 nM, (2) 200 pM and (3) 10 pM. Source/drain modulation: a 3 Hz sine wave with a 30 mV amplitude at zero DC bias. f) Conductance-versus-time data recorded after alternate delivery of 1 mM phosphate buffer and the following PSA solutions with AC excitation (0.5 V, 200 Hz). The order of PSA delivery: (1) 10 pM, (2) 40 fM and (3) 2 fM. Source/drain modulation: a 79 Hz sine wave with a 30 mV amplitude at zero DC bias.

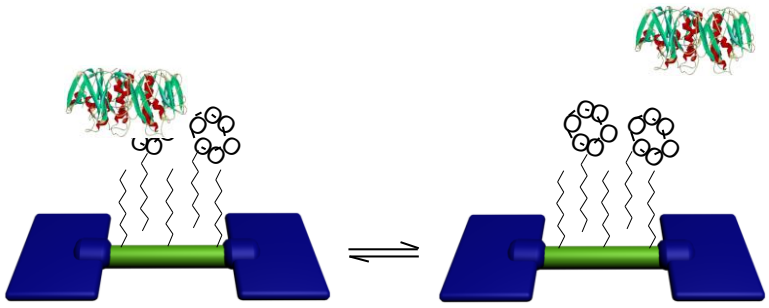

Scheme 2. Schematic of CTB binding and unbinding on Si NW sensor surface, where the hydrocarbon chains of gangliosides insert into the silane monolayer via hydrophobic interaction.

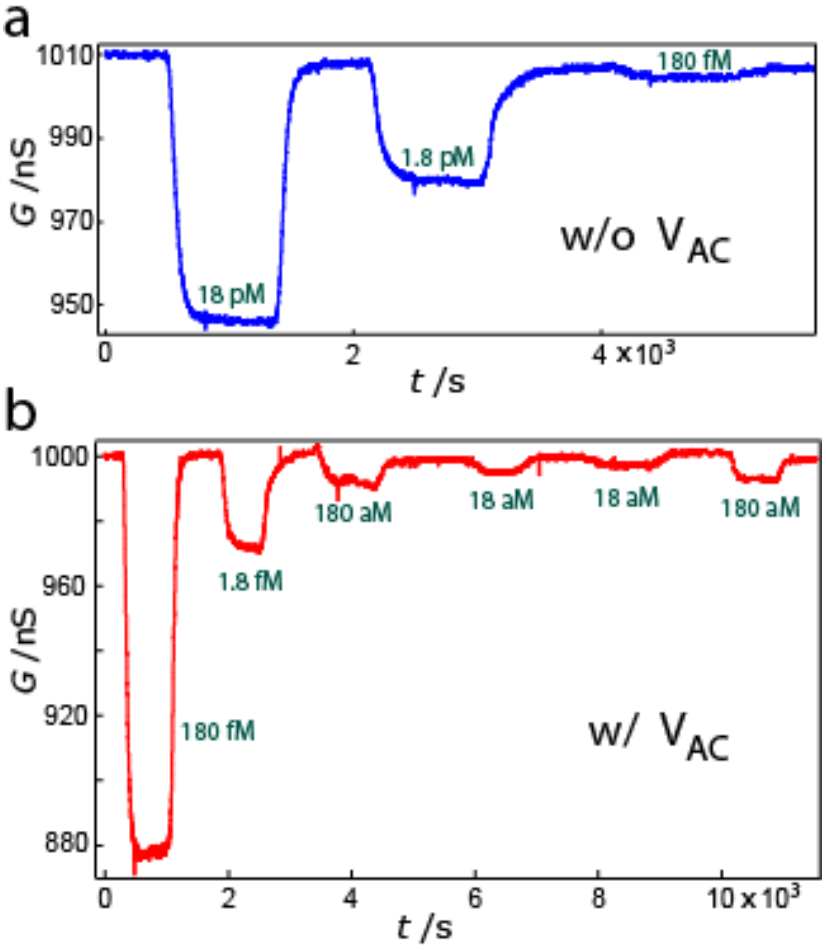

Figure 3. Real-time detection of CTB binding. a) Conductance-versus-time data recorded after alternate delivery of buffer and the following CTB solutions without AC excitation. The order of CTB delivery: (1) 18 pM, (2) 1.8 pM and (3) 180 fM. Source/drain modulation: a 3 Hz sine wave with a 30 mV amplitude at zero DC bias. b) Conductance-versus-time data recorded after alternate delivery of phosphate buffer and the following CTB solutions with AC excitation (0.5 V, 47 Hz). The order of CTB delivery: (1) 180 fM, (2) 1.8 fM, (3) 180 aM, (4) 18 aM, (5) 18 aM and (6) 180 aM. Source/drain modulation: a 79 Hz sine wave with a 30 mV amplitude at zero DC bias.

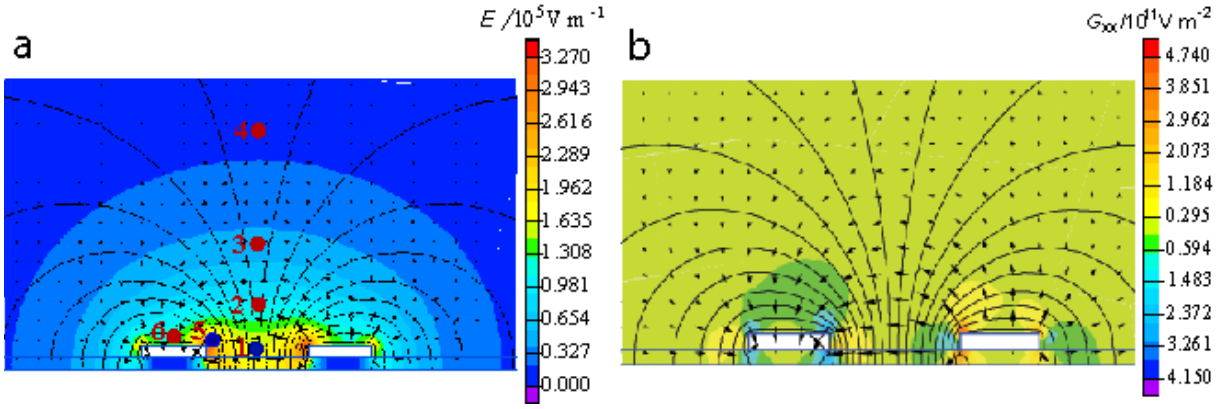

Figure 4(S2). (a) Field strength and (b) field gradient near the electrokinetic electrodes from two-dimensional electrostatic simulations (Quickfield, Tera Analysis, Denmark). Positions of the electric field measurement in (a): 1) X = 0, Y = 0 (in the middle of the electrode pair gap on the substrate; 2) X = 0, Y = 2.5 μm; 3) X = 0, Y = 5 μm; 4) X = 0, Y = 10 μm; 5) electrode edge; 6) electrode center. The order of field strength at the specific position: 5 > 1 > 6 > 2 > 3 > 4.

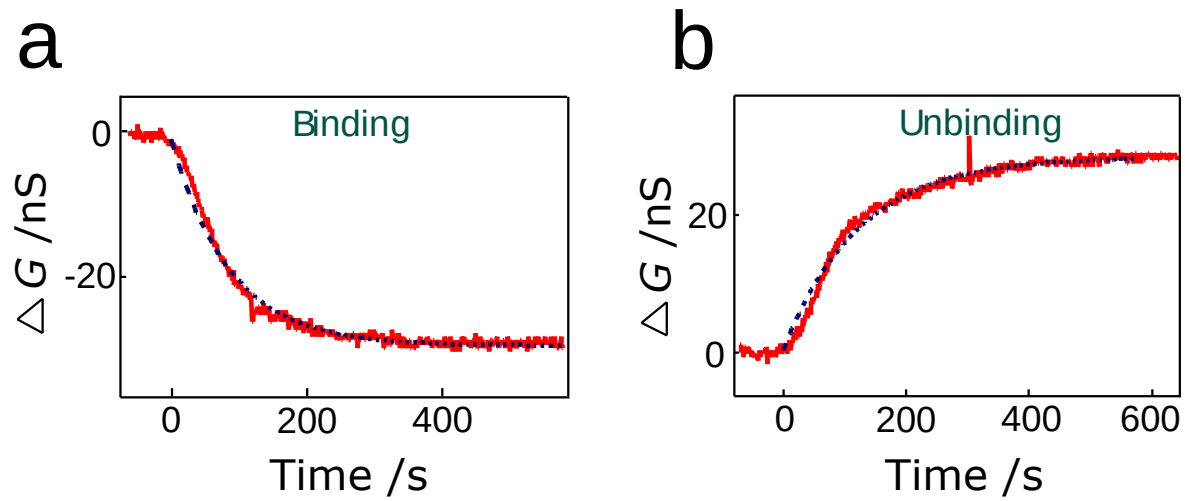

Figure S1. Kinetic analysis of curve fitting for CTB binding and unbinding with an expanded x-scale. (a) Binding and (b) unbinding curve (blue dotted lines) of 1.8 fM CTB with AC excitation. Single exponential fitting is used to fit the curve.